Assessment of coastal geomorphological changes using multi-temporal satellite derived bathymetry

Ankita Misra, Balaji Ramakrishnan

PII: S0278-4343(20)30168-0

DOI: https://doi.org/10.1016/j.csr.2020.104213

Reference: CSR 104213

To appear in: *Continental Shelf Research*

Received Date: 27 December 2019

Revised Date: 19 May 2020

Accepted Date: 31 July 2020

Please cite this article as: Misra, A., Ramakrishnan, B., Assessment of coastal geomorphological changes using multi-temporal satellite derived bathymetry, *Continental Shelf Research* (2020), doi: https://doi.org/10.1016/j.csr.2020.104213.

Assessment of coastal geomorphological changes using multi-temporal satellite derived bathymetry

Ankita Misra[1], Balaji Ramakrishnan[1]

1 Department of Civil Engineering, Indian Institute of Technology- Bombay, Mumbai, India, ankitamisra1987@gmail.com, rbalaji@iitb.ac.in

Corresponding Author:

Dr. Balaji Ramakrishnan, Associate Professor, Department of Civil Engineering, IIT Bombay, Powai, Mumbai -400076, Ph.: (+91) 2225767321, Email: rbalaji@iitb.ac.in

Abstract

The present study demonstrates the usability of Satellite Derived Bathymetry (SDB) to understand the geomorphological changes that have occurred in a coastal region located along Puducherry, India, where a beach restoration project was taken up in 2017 to arrest the shoreline erosion that is prevalent due to installation of hard structures. In the study, multi-temporal bathymetry data is generated by applying a non-linear machine learning technique of Support Vector Regression (SVR) on Landsat 8 OLI satellite dataset of 30m resolution. The empirically driven SVR is calibrated and validated using eco-sounder data collected during field measurement campaigns and fairly accurate SDBs with Root Mean Square Errors and Mean Absolute Errors ranging between 0.40-1.07m and 0.31- 0.85m, respectively are obtained. Subsequently, the derived temporal depth maps are studied to understand the morphological changes that have occurred in this coastal stretch and the results clearly show the development of a beach, north of the pier, followed by the stabilization of the coastline. The outcomes are further validated through an independent ArcGIS- DSAS based shoreline change analysis which suggests similar trends of accretion and erosion as observed through the bathymetry change analysis. The study thus substantiates that the beach restoration step has yielded positive results between 2017-2018 and throws light on the significance of SDBs in coastal monitoring, modelling and assessment.

Keywords – Multi temporal, Geomorphology, Nearshore bathymetry, Support Vector Machines, Landsat 8 OLI, Optical Remote Sensing,

1. Introduction

Accurate and updated coastal bathymetry is one of the most essential requirements for studies pertaining to the marine environment. The bustling anthropogenic activities along the coastal regions, as well as the effect of climate change in these areas, urges the development of accurate numerical models that can effectively estimate the coastal dynamics. Bathymetry is one of the primary inputs for driving the coastal models, and thus, there is a need to ensure the availability of detailed depth information at varying temporal and spatial scales. In-situ measurements of depths become challenging by virtue of the acquisition costs involved in deploying conventional methods, such as ship-based echo-sounding and LiDAR based techniques. In recent times, bathymetry estimation is carried out using drones coupled with Structure from motion (SfM) and fluid lensing technology (Chirayath and Earle, 2016; Casella et al., 2017; Purkis, 2018). Although drone-based depth mapping can enable centimetre scale resolution, it is prone to spatial coverage issues as it is constrained only to small areas due to technical limitations. Additionally, all the above techniques face logistical difficulties in case of repeated in-situ measurements, which is an important requirement for coastal monitoring and assessment. Hence, satellite-based remote sensing techniques offer an efficient alternative to SONAR, LiDAR and drone-based bathymetry as they enable coastal monitoring and reconnaissance at varying spatial and temporal scales as well as is more viable due to synoptic coverage and wide availability of datasets.

Spectrally based depth estimation algorithms used to obtain satellite-derived bathymetry (SDB) based on optical satellite imagery are broadly classified into physics-based models and empirical models (EMs), the latter being more widely used in literature. The first class encompasses the inversion of radiative transfer models and accounts for the physics involved in the interaction of light with the water surface, water column and bottom (Maritorena et al., 1994; Lee et al., 1999; Brando et al., 2009; Kerr and Purkis, 2018). The physics-based models essentially do not require in-situ measurements for calibration. According to Bierwith et al. (1993), physics-based models are very robust to variations in bottom types and capable of deriving water depths and seafloor reflectance simultaneously. However, the major drawback in case of these models is the need for intense atmospheric correction (Hedley et al., 2016) which as mentioned by Lyzenga et al. (2006) limits the accuracy of these models,

with root mean square errors of ≤ 1-2 m especially in shallow waters of depths less than 20m. Empirical models, on the other hand, provide regression-based estimates of depths, i.e. they use direct in-situ measurements in a study area to calibrate reflectance to depth relationship (Lyzenga, 1978; Philpot, 1989). Gao (2009) discusses the various remote sensing-based methods of bathymetry estimation with a special focus on optical remote sensing (ORS) technique and suggests that empirical methods of bathymetry retrieval are relatively advantageous than the other models (Benny and Dawson, 1983; Spitzer and Dirks, 1986) by virtue of their easy and quick implementation and computation speeds (Liu et al. 2015) . The most commonly used empirical algorithm is proposed by Lyzenga (1978, 1981), which is based on the Beer-Lambert law of absorption. The disadvantage of the linear algorithm is the assumption of a linear bottom type, which is later addressed through a ratio-based algorithm proposed by Stumpf et al. (2003). Both these regression models are reported to have reasonable accuracies in depth retrieval. In a review of the different imaging and non-imaging models for deriving bathymetry information, Jawak et al., (2015) explains the optical remote sensing methods of depth of penetration (Jupp, 1988), linear transform (Lyzenga et al., 2006), ratio transform (Stumpf et al., 2003); microwave remote sensing method of wave tracing (Mishra et al., 2013) along with several case studies that describe the application of these models (Doxani et al., 2012 ; Deidda and Sanna, 2012; Liew et al., 2012; Jawak and Luis, 2015) on different satellite datasets varying in spatial and temporal resolutions. Furthermore, the recent literature on bathymetry studies suggest improvements through the use of data driven methods (DMM) that involves application of complex machine learning (ML) techniques like Artificial Neural Network, Support Vector Machine etc.(Wang et al. 2019, Ceyhun and Yalçın, 2010; Gholamalifard et al., 2013; Eugenio et al., 2015; Makboul et al., 2017, Misra et al., 2018).

Collin and Hench (2015) showed that neural network(NN) outperformed the ratio transform model and could accurately predict water depths with the RMSE of 2.44m. Liu et al. (2015) compared the multi-layer perceptron (MLP) and general regression network with the inversion model and regression tree, and found that MLP and GNN performed better than the latter methods with RMSEs in the range of 1.22 -2.23m. The results from the methods of Least square boosting (LSB), Bagging ensemble and Support Vector Machine (SVM) were reported by Mohamed et al. (2017) and the authors highlighted that the three machine learning techniques provided more accurate results than Lyzenga's global linear model (GLM) and Neural Network (NN). Random forest technique was utilized by Sagawa et al. (2019) to derive a generalized depth estimation model for depths between 0-20m for five test

areas. Their model provided results (RMSE between 1.12- 2.43m comparable with those obtained from Lafon et al. (2002) and Lyzenga et al. (2006). Geyman and Maloof (2019) proposed an intermediate method between linear/ratio algorithms and machine learning called cluster-based regression (CBR) and reported that although the method is useful for mapping depths using a smaller dataset for a larger region, the method provides little or no improvement in comparison to the SVM. Yunus et al. (2019) thorough their study showed that the Random forest performed better than the empirical models, wherein the former resulted in depth predictions with RMSEs between 1.13-1.95m and the latter between 1.99m and 4.74. Based on the previous studies, it is evident that ML methods generally perform better than the existing empirical algorithms. The major advantage of the ML approaches is that they successfully account for the non-linearity that exists in the natural environment concerning the relationship between reflectance and depths and therefore, prove to be efficient in bathymetry retrieval as is demonstrated by Misra et al. (2018, 2019).

With this perspective, the present study utilizes the ML approach of Support Vector Regression (SVR) to derive Multi-temporal Satellite Derived Bathymetry (SDB) to understand geomorphological changes that have taken place in the coastal region of Puducherry, located in the East Coast of India. Generally, coastal erosion and accretion are regarded as natural processes, however, the introduction of man-made structures can considerably modify the wave direction and can lead to severe coastal erosion or/and accretion of a coastal region. Moreover, as mentioned by Van Rijn (2011) engineering structures essentially designed to protect shorelines can also lead to enhanced erosion in the adjoining area, which is a major problem of the Puducherry shoreline. Selvan et al. (2016) report the various structures that have been constructed along the coast of Puducherry during different periods, which include sea walls, ripraps, groins, and breakwaters. The Puducherry beach initially eroded due to the construction of the harbour that obstructed the natural flow of the sand from South towards the North. In the following years, short-term measures like construction of sea walls and groins were attempted by the Puducherry government, which however further intensified the erosion in the Northern portion. Consequently, as a part of a sustainable shoreline management plan, the government along with National Institute of Ocean Technology (NIOT, Chennai) in 2017 proposed a beach restoration project consisting of two components (1) construction of artificial reefs (2) beach nourishment, which started in March 2017.

The main objective of the present research is therefore to assess and report the geomorphological impact of this beach restoration project with the help of rigorously

calibrated and validated SDBs obtained from freely available Landsat 8 OLI medium resolution images (30 m). Additionally, a shoreline change analysis is also performed by using the Digital Shoreline Analysis System (DSAS) tool in the ArcGIS environment to evaluate the erosion/accretion patterns in this coastal stretch, in order to validate the results of the SDB based geomorphological analysis.

2. Study Area

The region considered for this study is a coastal stretch located along the city of Puducherry, an enclave of Tamil Nadu state, on the east coast of India. The coast experiences both south-west (SW) as well as north-east (NE) monsoon, the latter being more dominant. Moreso, by virtue of its geographical location the region experiences a higher frequency of cyclones as compared to the west coast of India (Kudale et al., 2004).

Mostly, low lying, the average elevation of Puducherry is about 15m above mean sea level with a number of sea inlets, referred to as ‘backwaters' intersecting the land. Barrier dunes/ Sand dunes are seen as continuous mounds and prominent estuarine mouths are witnessed along the coastal landscape. The average significant wave height along the coast is 0.9m with deep water waves reaching from South and Southwest during SW monsoon and from the northeast during NE monsoon. The average tidal range observed in this region ranges between 0.7–0.8m (Sandhya et al., 2014; Umesh et al., 2017). According to Neelamani and Sundaravadivelu (2006), the combined effect of waves, tides and winds generate currents that together drift about 1.0 million m^3 of sand from south to north and 0.4 million m^3 from north to south, in a year in this location.

In order to assess the geomorphological changes that have taken place by virtue of the shoreline management project (Figure 1(a)), a 3km coastal stretch (Figure 1(b), Red box,) is chosen as the study area. The dumping location of sediment is chosen to be near the pier, for this project. Since the analysis is conducted using a time series of Satellite Derived Bathymetry (SDBs) obtained by applying an optical based machine learning algorithm, hence turbidity is a very important consideration affecting the prediction accuracy of the estimated bathymetry. Bharathi et al. (2017) report that the transparency observed for this coastal region is higher during non-monsoon periods further decreasing in monsoon, with an average value of 5.4 ± 2.3m. The average Total Suspended Matter (TSM) observed for all seasons is 38.1 ± 21.8 mg/l. Hence, based on the visual interpretation of the satellite image as well as

the literature available, it is evident that region is dominated by clear waters and the depth ranges observed within this region lie between 0- 10m.

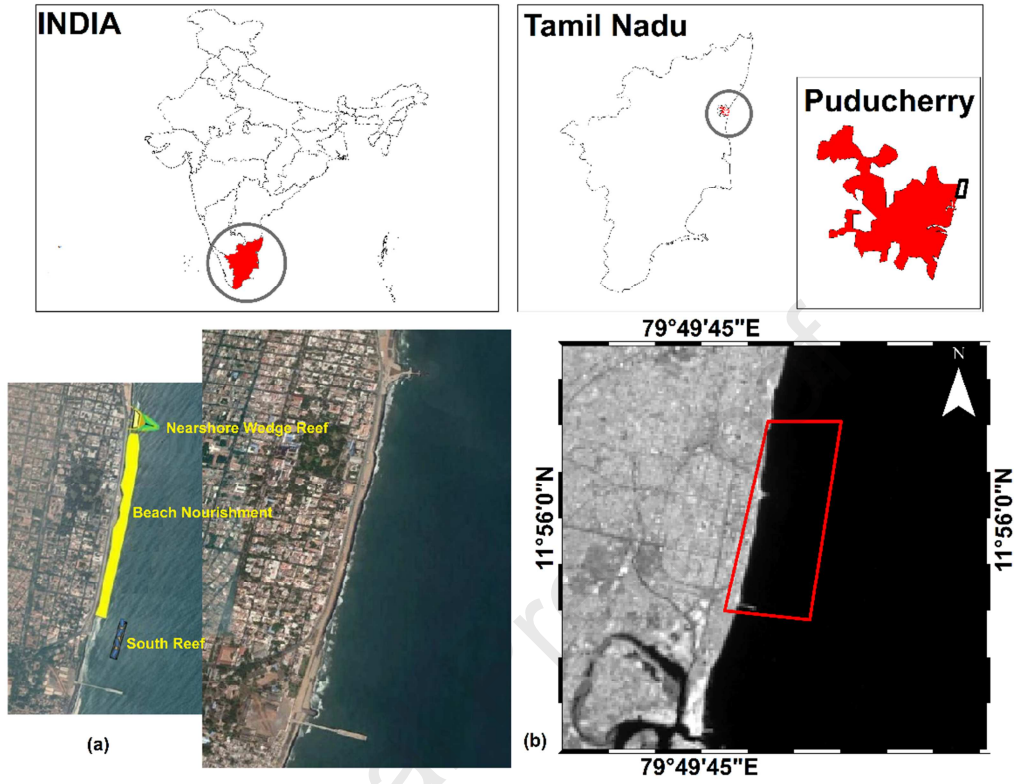

Figure 1 (a) Beach restoration plan depicted in Yellow (b) Location of Study area

3. Data and Methodology

3.1 Data – In situ measurements and satellite data

The depth information collected using the CEE – ECHO – High definition single beam eco-sounder(http://www.ceehydrosystems.com/products/single-beam-echo-sounders/cee-echo/#1511901053278-fdfe7119-b0bb) for the years 2015 and 2016, and for the different months of 2017 are used for the calibration and validation of the ML based bathymetry retrieval model. The XY positions of the measured data are projected to UTM zone 44 and the corresponding depths are tide adjusted to Mean Sea Level (MSL).

Further, based on the operational difficulty in conducting field campaigns concurrently with the satellite over pass, the best quality satellite datasets closest to the date of in-situ measurements are chosen. A series of Landsat 8 OLI imageries are used for assessing the

performance of SVR for the multi-temporal geomorphological analysis. Several studies have reported the use of Landsat 8 OLI for bathymetry estimation (Pacheco et al., 2015; Knudby et al., 2016; Vinayaraj et al., 2016; Kabiri, 2017; Pushparaj and Hegde, 2017, Makboul et al., 2017 and Yunus et al., 2019) as it has the adequate spectral and radiometric characteristics required for coastal water applications (Mobley et al. 2016). Furthermore, Hamylton et al. (2015) state that based on the capacity to relate in-situ measurements to satellite data, Landsat 8 OLI (or Sentinel 2 MSI) can produce comparable results to commercial sensors such as WorldView 2. This is also evident in a recent research by Cahalane et al. (2019) where datasets of different sensors Landsat 8 OLI, RapidEye and Pleiades are compared by applying the ratio transform model and it is observed that all the three datasets provide robust and meaningful results with comparable accuracies.

The in-situ data and the satellite images used for this study along with their attributes are enlisted in Table 1 . It is to be noted here that since the satellite images are procured at different time and date, corresponding tidal offsets are applied to the final obtained SDBs for comparison with in-situ measurements.

Table 1 List of data used and their attributes

In situ measurements			Satellite Imagery		Used For
Date	**Approx. Extent (Km^2)**	**Depth Range (m)**	**Date**	**Tidal Elevation (m)**	
February 2015	10	0 - 9.5	16 February 2015	0.94	Calibration
March 2016	1.7	0 -7.8	22 March 2016	0.56	Calibration
February 2017	2.5	0- 9.5	5 February 2017	0.93	Calibration
July 2017	2	0-10.0	12 May 2017	0.41	Validation
October 2017	2	0-9.5	19 October 2017	0.49	Validation
			7 January 2018	0.54	Prediction

3.2 Methodology

The methodology for obtaining SDBs primarily involves 3 steps - (i) Pre-processing of satellite imagery (ii) Spatial subsetting and Land/ water separation and (iii) Application of the bathymetry estimation algorithm. The following sections provide a detailed information about each step.

3.2.1 Pre-processing of Satellite Imagery

In this study Landsat 8 OLI datasets are used for the application of the depth retrieval algorithm. The ACOLITE atmospheric correction (AC) processing software developed by the Royal Belgian Institute of Natural Sciences is utilized in this analysis (Vanhellemont and Ruddick, 2018, Vanhellemont, 2019). ACOLITE uses Aerosol Optical Depth evaluation and automatic water surface discrimination for the atmospheric correction and sun glint removal and is specifically applicable for the AC of multispectral images of Landsat 8 OLI and Sentinel 2 MSI used for marine and inland water analysis (Vanhellemont, 2019; Vanhellemont and Ruddick (2014, 2015, 2016, 2018)).

3.2.2 Spatial Sub-setting and Land/water separation

Considering the Landsat 8 OLI calibration is reflectance based the Top of Atmosphere (ToA) reflectance is used for retrieval of the variables required for the ML based depth retrieval (Pahlevan et al., 2014). The reflectance images thus obtained are further utilized for spatial sub-setting.

An improved method suggested by El Kafrawy et al. (2017) is explored for separating the water pixels and shoreline extraction. The method combines two popular indices, of (1) Normalized Difference Vegetation Index (NDVI) and (2) Normalized Difference water index (NDWI) expressed as equation (1) and (2) respectively. The choice of this method is based on the study by Ma et al. (2013) who suggests that using NDVI and NDWI individually can lead to misclassification of the water features and hence combining the two can significantly improve the results.

$$NDVI = \frac{NIR-R}{NIR+R} \quad (1)$$

$$NDWI = \frac{NIR-G}{NIR+G} \quad (2)$$

where, *NIR* is Near infrared band reflectance, *R* is red band reflectance and *G* is reflectance in green band.

After the two indices are calculated, a thresholding process is applied to extract the features based on interpretation of the resultant images. The features delineated based on the optimum threshold values are represented as A(NDVI)and A(NDWI) and those extracted with higher threshold values are defined as O(NDVI) and O(NDWI). Further, by applying the relation (Ma et al. 2013) given by equation 3 the shorelines are delineated, followed by vectorisation which is conducted to extract the shoreline shapefiles. This process also enables efficient separation of the land and water pixels, where the latter is used to apply the depth retrieval algorithm.

$$(O\ (NDVI) \cup A(NDWI) \cap\ O\ (NDWI) \tag{3}$$

3.2.3 Bathymetry Retrieval Algorithm

EMs are widely employed for bathymetry estimation; however, they are limited in case of handling complex and non- linear relationships between independent and dependent variables, particularly in coastal environments with increased turbidity. ML techniques capture this non-linearity more efficiently and thus have the potential to improve the traditional multivariate regression models with better prediction accuracy (Mohammad et al. 2016). The present study therefore involves the application of data-driven machine learning approach for depth estimation.

Optimal Input Parameter selection

It is imperative, nevertheless, to understand that the selection of the input parameter or parameters, is the most important step before the application of any algorithm for bathymetry retrieval. This can be either single band, multiple bands, ratio of bands or a combination of all or some parameters. Case studies based on the Lyzenga model suggest the use of multiple bands with multi regression and those based on Stumpf model utilize the ratio of the lower absorption band to the higher absorption band for linear regression. In most case studies, the ratio of blue by green band is used as an input for the empirical analysis. This is based on the principle that the best spectral bands are selected depending on their capability of penetrating water, and mostly spectral bands of short wavelength are chosen. However, Leglieter et al. (2009) suggests the optimal band ratio analysis (OBRA) for choosing the best ratio as input

to the regression model instead of directly choosing the blue/green ratio. Contrary to this, a research proposed by Jadidi et al. (2018) advocates the use of Multiple Optimal Depth Predictor Analysis (MODPA) which combines various depth predictors (Lyzenga or Stumpf) along with intensity component of the Hue-Saturation-Intensity (HSI) colour space transformation to derive depths <1m.

Here, the four Landsat 8 OLI bands of coastal blue, blue, green red are considered for choosing the best parameter for bathymetry estimation along the coast of Puducherry. The coastal blue is an additional band in comparison to Landsat ETM+ and thus is included in the assessment. The other three bands are considered based on the study by Gao (2009) which reports that in clear waters, where little backscattering takes place and radiation can penetrate deeper waters, short wave algorithms are desirable, whereas, in case of turbid waters, there is a shift in the optimum wavelength and the water depths correlate with red band.

On comparing the individual bands, it is observed that the blue, green and red bands show better correlation than the coastal blue band and when the band ratios are considered, the best correlation of 0.99 is obtained in the case of blue/green ratio (Table 2). As there are several parameters with good correlations, a step-wise regression is conducted to derive the optimum predictors. The step-wise regression is a systematic approach to retain or eliminate predictors from a linear model based on their statistical significance in explaining the variable to be predicted, which in this case is nearshore bathymetry. Unlike MODPA discussed by Jadidi et al. (2018), use of high dimensional predictors, such as HSI are refrained in this study as they need to be evaluated additionally, pose a threat of over-fitting and can result in redundant or correlated predictors which can reduce the accuracy of the regression model.

Finally, based on the above analyses, two scenarios are obtained - (1) using blue/green ratio as a single predictor (2) or using a combination of the predictors obtained by stepwise regression. Both these scenarios, as well as for completeness, a third scenario with all the bands and ratios combined, are considered to run the ML model to arrive at the best parameter model that can be used to derive time varying depth maps.

Table 2 Correlation analysis for choosing the best input parameter

Satellite bands and ratios	Coefficient of determination (R^2)
Coastal blue (cb)	0.79
Blue (b)	0.83
Green(g)	0.95
Red (r)	0.95
Coastal Blue/Blue	0.94
Coastal Blue/Green	0.98
Coastal Blue/Red	0.96
Blue/Green	0.99
Blue/Red	0.96
Green/Red	0.53

Depth Retrieval Algorithm

Support Vector Regression is the ML technique chosen for depth retrieval for the optical satellite datasets. Considering the technique does not directly consider the environmental factors affecting the reflective properties of the water column, it can be considered as an efficient method for bathymetric mapping over the previously used regression models. The analysis conducted here involves utilizing a small dataset for multi-temporal prediction of depths. SVR is reported to perform well in data scarce conditions in comparison to methods like ANN or Random Forest which usually require a huge amount of observation to get a good convergence. The SVR approach attempts to learn the input-output relationship by solving a quadratic programming problem. It is a method to estimate a function that maps from an input object to a real number based on training data and essentially has the same properties of margin maximization and kernel trick for non–linearization similar to classifying SVM (for a more detailed understanding of SVR, readers are referred to Smola and Scholkopf (2004)).

The general expression for a regression based SVR model (Misra et al., 2018) is as follows –

$$E = \sum_{i=1}^{p} L_{si} + \lambda_{RT} \|Pf\|^2 = \sum_{i=1}^{p} L_{si} + \Omega(h, l) \quad (3)$$

where,

E is commonly referred to as a cost or generalisation error function to measure model's performance, goodness of fit;

L_{si} denotes the closeness to data, i.e., the sum of differences between the measurements and model outputs calculated in the training phase;

p refers to the size of measurements/training data;

Ω is the VC (Vapnik and Chevornenkis) function (also called as confidence term or confidence interval) and relates to the smoothness of approximation;

λ_{RT} denotes the regularisation parameter (i.e., the Lagrange multiplier);

h is the VC dimension;

l refers to the number of support vectors.

In case of SVR, the optimization problem is called a convex problem, whereby given a covariance function the solution is unique and can be found efficiently. This is again more advantageous than the other non- linear prediction technique (in particular neural networks) which are prone to local minima (Vapnik 1995) or random forests which can result in overfitting. The SVR model requires two training parameters C and ε, the former being the penalty parameter that specifies the trade-off between the training error and the Vapnik-Chervonenkis dimension of the model; and the latter is called the insensitive loss function which controls the number of support vectors enabling data compression as well as smoothing of noisy data (Vojinovic et al., 2013). The following step involves the non-linearization of the model which is achieved by applying a function that takes the training vectors from a low dimensional input space and transforms it to a higher dimensional space. This transformation is referred to as the kernel function and is represented by $k(x, x')$ where x and x' are each input data vectors. In the present study the Radial Basis Kernel function (RBF) or Gaussian Kernel (Zhihua and Honglian, 2012) is used which is expressed as follows-

$$K_{RBF}(x, x') = exp\ exp\left(-\gamma \|x - x'\|^2\right), \gamma > 0 \quad (4)$$

pre

where, γ, is the Gaussian function; x, x' are feature vectors.

Multi-temporal Geomorphological Change Analysis

Following the selection of the best predictor SVR model and validation, depth maps at 30m resolution are generated using Landsat 8 OLI datasets to understand the impact of the beach restoration project taken up by the government on the coastal morphology of this region. The change in the bathymetry between the different months of the year 2017 are evaluated and the results are reported. The outcomes of this assessment are further validated with the help of an independently executed shoreline change analysis as explained further.

Digital Shoreline Analysis System (DSAS) based Analysis

In order to estimate the temporal variations in shoreline positions for the same months considered for the geomorphological analysis, the Digital Shoreline Analysis System (DSAS) tool that works within the framework of Environmental Systems Research Institute (ESRI) Geographic Information System (ArcGIS 10.2) software is utilized to substantiate the results of the SDB based analysis. DSAS is a computer software that computes rate-of change statistics from multiple historic shoreline positions available in the GIS environment. (Thieler et al. 2005). The shoreline positions are extracted using a method suggested by El Kafrawy et al. (2017) as illustrated in section 3.2.2. Finally, the raster to vector function is used to derive the shorelines in the vector format (.shp) which is then used as input to DSAS to calculate the rate of change. This is achieved by setting up transects at every 150m of the baseline created parallel to the shoreline, along the 3km coastal stretch considered for this analysis. The DSAS tool estimates the Net Shoreline Movement (NSM) and End Point Rate (EPR) wherein NSM is the distance between the oldest and the youngest shoreline for each transect and the EPR is obtained by dividing the NSM by the time elapsed between the two shoreline positions.

4. Results and Discussion

4.1 Bathymetry Retrieval using Optical Remote sensing

4.1.1 Optimal SVR Model and Parameters

The SVR technique applied in this study is an empirical approach and requires field measurements for training the model. For any machine learning approach, it is imperative to ensure that the input data is structured in a way that it helps the model to learn and develop a relationship between the independent and dependent variable, and in this case, between image reflectance and depths successfully. According to Martens and Dardenne (1998) an important key to ML based bathymetry retrieval is to have sufficient number of representative samples for calibration of the model mainly to ensure that the regression captures the variability and complexity of the data well. As the robustness of the SVR depth model greatly depends on a well processed training data, here, in-situ data of February 2015, March 2016 and February 2017 are combined for preparing the calibration dataset. The other available field datasets of July and October 2017 are solely utilized for validation of the SVR model. Subsequently the combined data, created by collating the data of the mentioned three years are divided into training (80%) and testing (20%) datasets (Table 3) in order to test the three predictor scenarios considered in section 3.2.3, and hence, arrive at the best SVR based depth prediction model for further validation.

Table 3 Statistics of the training and test datasets

	No. of Data Points	Minimum Depth(m)	Maximum Depth (m)	Mean Depth (m)
Training Phase	834	0.02	10.41	5.18
Testing Phase	208	0	10.36	5.29

It can be observed in Table 4 that the blue/green ratio SVR model provides the best depth estimation as compared to the other predictor models. The b/g model uses a training dataset of 834 points as an input to train the SVM model for estimating depths along the coast of Puducherry. About 32.85% of this training dataset is selected as support vectors when the C and ε values chosen are 1000 and 0.1 respectively, resulting in a training error of 3.22%. On testing the model with 208 data points, a low-test error of 2.55% is obtained. The comparison of the testing dataset with the in-situ measurements yields a correlation of 0.99. Subsequently, based on the good performance of this model, it is further used to estimate depths for all the satellite datasets with available corresponding in-situ measurements.

Table 4 Results obtained for different predictor scenarios and SVR

Scenario	Predictor Variable	R^2	RMSE (m)	MAE (m)
Scenario (1)	b/g	0.99	0.13	0.09
Scenario (2)	b+g+r+(b/g)+(b/r)+(g/r)	0.98	0.32	0.14
Scenario (3)	Cb+b+g+r+(cb/b)+(cb/g)+(cb/r)+(b/g)+(b/r)+(g/r)	0.98	0.39	0.16

4.1.2 Validation of SVR based depth retrieval and multi-temporal bathymetry maps

This section reports the validation results that are obtained on the application of the SVR model with the chosen set of training data and model parameters to the datasets of February 2015, March 2016, February 2017, May 2017 and October 2017. The primary objective of carrying out a detailed validation study is to demonstrate the competency of this approach in deriving depth maps with limited training data over a longer temporal span. This is mainly to ascertain whether satellite derived bathymetry can aid in decreasing the requirement of carrying out repetitive in-situ measurements for time varying coastal studies.

Two aspects need to be noted here, firstly, there is no Landsat Imagery available corresponding to the July 2017 in-situ measurements, hence the imagery of May 2017 is utilized for carrying out the validation; secondly, the in-situ measurements of July 2017 and October 2017 have not been included in the preparation of the training dataset and hence, they form independent validation sets for this model.

In order to assess the prediction accuracy, Satellite-Derived Bathymetry (SDB) maps are compared with that of the in-situ measurements obtained by using echo-sounder. The residual statistics between the satellite-derived depths (Z_{sat}) with the corresponding echo-sounding measurements (Z_{echo}) are reported along the various descriptive statistics like bias, difference

median, Root Mean Square Error (RMSE) and Mean Absolute Error (MAE). In the case of the datasets used for training, the univariate statistics for each, individually, are given in Table 5. It is evident that the SVR model has performed fairly well for all the three datasets of the different years in spite of the spatial variability of the in-situ measurements. This encourages the application of SVR to obtain SDB, even when a limited amount of in situ measurements are available.

Table 5 Error statistics obtained by comparing predicted and observed value of depths in meters for the training datasets of February 2015, March 2016, February 2017

Statistical Parameters	Feb-15		Mar-16		Feb-17	
	Z_{echo}	Z_{sat}	Z_{echo}	Z_{sat}	Z_{echo}	Z_{sat}
Number of data points	96840		5341		16019	
Min (m)	0.00	0.00	0.00	0.04	0.02	0.44
Max (m)	10.41	12.07	7.80	7.21	9.57	9.11
Mean (m)	6.68	6.98	5.04	4.96	5.64	5.47
Median (m)	7.15	7.58	5.46	5.57	6.03	5.44
Standard Deviation (m)	2.28	2.64	1.85	1.85	1.95	1.61
Bias (m)	-0.30		0.08		0.17	
Dif(Median) (m)	-0.43		-0.11		0.59	
R^2	0.85		0.96		0.85	
RMSE (m)	1.07		0.40		0.79	
MAE (m)	0.85		0.31		0.59	

For the independent datasets, in order to ensure an in-depth analysis of the strengths and limitations of the SVM model as well as to gain an understanding of the uncertainty within specific depths, a statistical analysis is conducted by dividing the depths into classes of 2m ranges. The performances of the models in depicting the nearshore bed profiles are also assessed, with 12 transects from a baseline (B1) spaced every 150m (T1 to T12) and compared with that obtained from in situ measurements. Complementing this, difference maps (Stauble 1998) computed by subtracting the SDB values from the echo-sounding measurements are also generated. The Difference Map Method (DMM) calculates the vertical variations in cells by calculating the difference between two raster surfaces and enables the assessment of the spatial distribution of error associated with the bathymetry estimation. The DMM approach is applied here by interpolating both the raster surfaces to 30m resolution.

As stated before, the depth estimations based on the May 2017 imagery is compared with the in-situ measurements conducted in the month of July 2017 due to the unavailability of cloud-free satellite imagery for the later date. It is obvious that a good agreement between the echo-sounding measurements and the SDB depths cannot be expected, due to the seasonal, or

morphological changes caused by the presence of the artificial structures. Although, the coefficient of determination (R^2) obtained after considering the entire depth is 0.93, this difference in the dates of the observed and predicted values has resulted in large errors which is evident from the high value of bias (-0.97m) obtained for the entire considered depth range. The SVR is observed to predict well in-depth ranges of 0-2m and 4-8m with the MAE ranging between 0.45-0.70m (

Table ***6***). Contrary to this, for depths between 2-4m, the model is observed to have larger errors with a high bias value of -0.75m, which may be attributed to the continuous wave breaking in the swash zone (Pacheco et al. 2015). The highest bias of 0.80m is observed for the depth range of 8-10m.

Furthermore, based on the DMM (Figure 2) it is observed that approximately 88% of the resultant SDB has a difference lying between -1 and +1m. The greater differences in the predicted values are seen in the nearshore region, which, however, constitutes only 12% of the entire dataset. The capability of the model in estimating depths is further confirmed through the comparison of transect-based sea bed profiles as can be seen in Figure 3 and Figure 4, where good agreement of the predicted depths with the in-situ measurements are observed for majority of the transects.

Table 6 Depth –wise error statistics for the validation datasets of May 2017

	May-17											
Statistical Parameters	**0-2**		**2-4**		**4-6**		**6-8**		**8-10**		**Overall**	
	Z_{echo}	Z_{sat}	Z_{echo}	Z_{sat}	Z_{echo}	Z_{sat}	Z_{echo}	Z_{sat}	Z_{echo}	Z_{sat}	Z_{echo}	Z_{sat}
Number of Data Points	397		1465		2993		5366		2885		13106	
Min (m)	0.21	0.26	2.00	0.82	4.00	2.58	6.00	4.66	8.00	6.58	0.21	0.26
Max (m)	1.99	2.83	3.99	4.92	5.99	6.62	7.99	8.21	9.67	8.32	9.67	8.32
Mean (m)	1.33	1.35	3.14	2.48	5.12	4.51	7.08	6.72	8.56	7.70	6.34	5.79
Median (m)	1.42	1.35	3.23	2.46	5.18	4.55	7.12	6.76	8.50	7.80	6.77	6.39
Standard Deviation (m)	0.48	0.53	0.57	0.70	0.57	0.87	0.55	0.75	0.38	0.33	1.96	1.96
Bias (m)	-0.07		-0.75		-0.67		-0.40		-0.80		-0.97	
Dif(Median) (m)	0.07		0.21		0.63		0.36		0.70		0.38	
RMSE (m)	0.55		0.87		0.80		0.63		0.93		0.77	
MAE (m)	0.45		0.78		0.70		0.50		0.86		0.66	

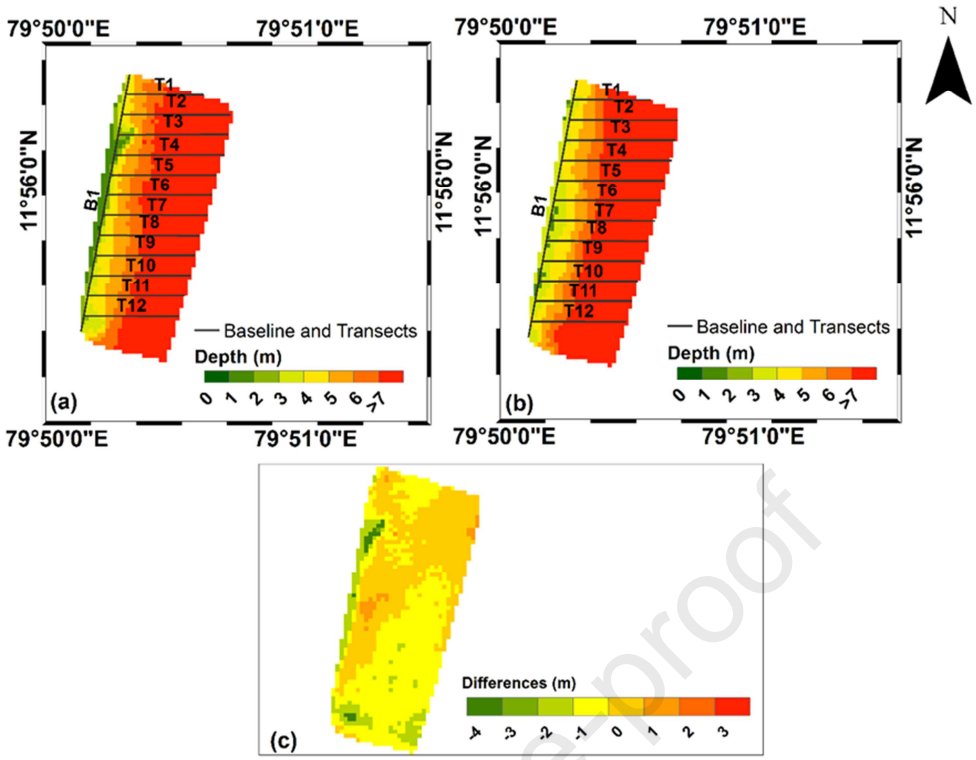

Figure 2 Comparison of bathymetry map obtained using (a) In-situ measurement of July 2017(b) Landsat OLI imagery of May 2017 showing baseline B1 and transects (T1-T12) spaced every 150m (c) DMM map between in situ measurement and SDB

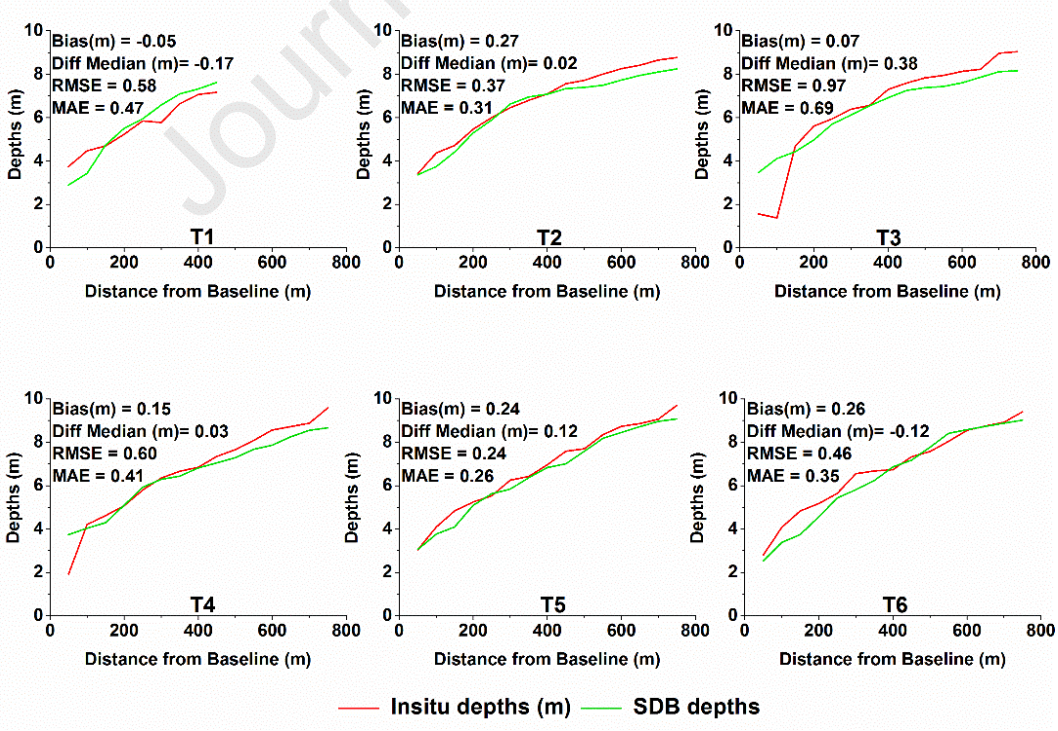

Figure 3 Comparison of near-shore seabed profiles of May 2017 for transects T1-T6

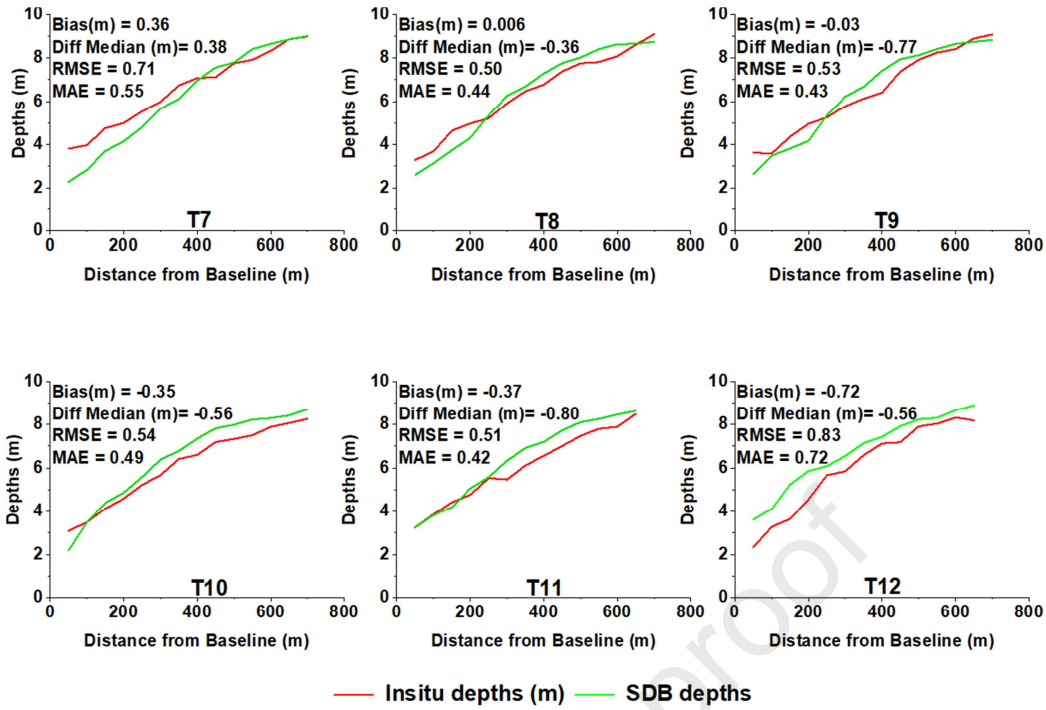

Figure 4 Comparison of near-shore seabed profiles of May 2017 for transects T7-T12

For October 2017 dataset, a total number of 187466 data points (Table 7) are validated with in-situ measurements. In this case, the model over-estimates in the lower depth class of 0-4m and is in fair agreement with in-situ values for 4-10m, a trend similar to that observed in the case of May 2017. This trend concurs with earlier studies (e.g. Pacheco et al., 2015, Traganos et al., 2018) that report an over-prediction in shallow depths and an under prediction in greater depths. According to Stumpf et al. 2003 the higher errors in the deeper waters is caused due to the high absorption and scattering of light in the greater depths. However, the classes of lower accuracy constitute only about 30% of the entire dataset, whereas the rest of the 70% data are obtained with better accuracies (RMSE < 1m).

In addition, it is interesting to observe that the SDB can capture the beach nourishment procedure (Figure 5). All the transects for this imagery (Figure 6, Figure 7) show RMSE value =<1m except T12, which is closer to an existing pier structure (location of nourishment), that has the highest RMSE and MAE values of 1.02m and 0.86m respectively. The other transects showing higher error values are T1 and T3 and those showing the maximum agreement are T4-T5. It is evident from the results that the model appears to overestimate in most of transects. The bias and Difference Median values obtained for this dataset is relatively small, with the lowest values being for the depth ranges between 4-6m, which also show the lowest value of RMSE and MAE. The highest inaccuracies are observed

for the depth class of 8-10m, a trend similar to that seen in the case of May 2017 imagery. This highlight the intrinsic limitation of optical remote sensing-based approaches i.e. with the increase in depth the accuracy decreases.

In the DMM derived from the subtraction of in-situ measurement based resampled 30m raster and the SDB, it is observed that about 75% of the residuals lie between -1 to 1m. Greater values of RMSE between -2 to -3m and > -3m cover 24% and 1% of the dataset respectively. The larger RMSE and MAE can be accounted to two factors, firstly, in case of October 2017 imagery, a large number of data points are predicted using a small training set; secondly, the temporal interval between the training points and this dataset is relatively greater, and generally forecasting accuracies decrease with the increase in the time interval (Rana and Koprinska, 2016). Moreover, the increased amount of suspended sediment in the water column may have also resulted in inaccuracies in prediction. Nevertheless, an overall R^2 of 0.91, RMSE error of 0.89m and MAE of 0.71m are significantly acceptable results that are relevant from the viewpoint of utilizing SDBs for practical coastal studies.

The main advantage of using ML approaches over traditional empirical methods is that the model free structure of these algorithms enables reducing the number of repetitive in- situ measurements which is an essential perquisite for coastal monitoring. As mentioned by Solomantine et al (2009), ML methods mainly involve finding the appropriate connections between the system's input and output variables (reflectance, depth) and do not explicitly require the knowledge of the physical behaviour of the system. Hence, these techniques prove to be a major advancement over the conventional empirical techniques. With this viewpoint, for the application of SVR here, an attempt has been made to deal with the turbidity problem by collating data of previous years as training set, so that it is capable of representing variable conditions. However, since the SVR model depends on the spectral characteristics of the satellite image it does suffer from limitations caused due to turbidity. This region is essentially a clear water region as is mentioned in section 2, nevertheless, sand replenishment can introduce turbid conditions which leads to higher inaccuracies as is evident in the statistics of May and October 2017 datasets. A few studies address the turbidity problem by utilizing optical remote sensing data and wave-based approaches which applies the linear dispersion equation, but yet again these methods are limited in case of absence of visible swells in the imagery or presence of clouds (Mancini et al., 2010; Danilo and Melgani, 2016; Danilo and Melgani, 2019). In terms performance of SVR in varied environmental conditions, a study conducted by Misra et al. (2018) reports that this technique performed well in the case of both non- turbid and turbid conditions of the Dutch Sint Maarten Island

and the Ameland Inlet and produced RMSE errors of 0. 69m and 0.34m respectively. Similarly, in an interesting study by Mohamed et al. (2017), the performance of Support Vector Machine, Bagging and Least Square Boosting was compared for bathymetry retrieval in 3 different study regions with varying depth ranges. The accuracy for all the three algorithms ranged between 0.65m – 1.11m RMSE. Based on the literature review (refer section 1) conducted during this research it is evident that there are several ML approaches available for bathymetry estimation and a comparative assessment between them shows that the performance of each ML technique varies based on the characteristics of the study area (water quality, bottom type), pixel size of the satellite image, the considered depth ranges and the availability and number of in-situ points. Resultantly, unless similar conditions are available, an evaluation of the relative performance of the various ML methods is not completely possible. Nevertheless, on assessing the accuracies observed by different researchers in various study regions and those obtained from the validation analysis in this study, it can be inferred that SVR method with appropriate parameters can be used for generating multi-temporal depth maps even in the cases of limited availability of in-situ measurements. Furthermore, it is also capable of forecasting depths in scenarios when no field measurements are available. It is important here to understand that irrespective of the potential of the bathymetry retrieval algorithm utilized, optical remote sensing in general is constrained in seasonal conditions of unfavourable weather as it becomes very difficult to procure cloud free good quality data. The all-weather capability of SAR can prove to be an efficient alternative in this case. SAR retrieves bathymetry measurements based on its interaction with the seabed morphology sensed as sea surface roughness. However, utilizing SAR is possible only for depth ranges between 10-70m (Pleskachevsky et al., 2011) and therefore out of the scope of this analysis.

592

593

594 **Table 7 Depth –wise error statistics obtained for the validation datasets of October 2017**

October-17												
Statistical Parameters	**0-2**		**2-4**		**4-6**		**6-8**		**8-10**		**Overall**	
	Z_{echo}	Z_{sat}	Z_{echo}	Z_{sat}	Z_{echo}	Z_{sat}	Z_{echo}	Z_{sat}	Z_{echo}	Z_{sat}	Z_{echo}	Z_{sat}
Number of Data Points	15788		33734		50410		69435		18099		187466	
Min (m)	0.04	0.23	2.00	1.17	4.00	3.02	6.00	4.51	8.00	6.51	0.04	0.23
Max (m)	1.99	3.46	3.99	5.37	5.99	7.05	7.99	7.39	9.04	7.56	9.04	7.56
Mean (m)	1.40	2.11	3.11	3.76	4.99	4.92	7.09	6.35	8.27	7.05	5.43	5.21
Median (m)	1.43	2.24	3.18	4.01	5.02	4.86	5.02	4.86	8.25	7.07	5.77	5.46
Standard Deviation (m)	0.39	0.67	0.61	0.78	0.60	0.57	0.56	0.49	0.19	0.17	2.11	1.53
Bias (m)	-0.71		-0.65		0.07		0.72		1.22		0.22	
Dif(Median) (m)	-0.80		-0.83		0.16		0.74		1.17		0.30	
RMSE (m)	0.92		0.88		0.48		0.66		1.23		0.81	
MAE (m)	0.82		0.79		0.37		0.58		1.22		0.71	

595

596

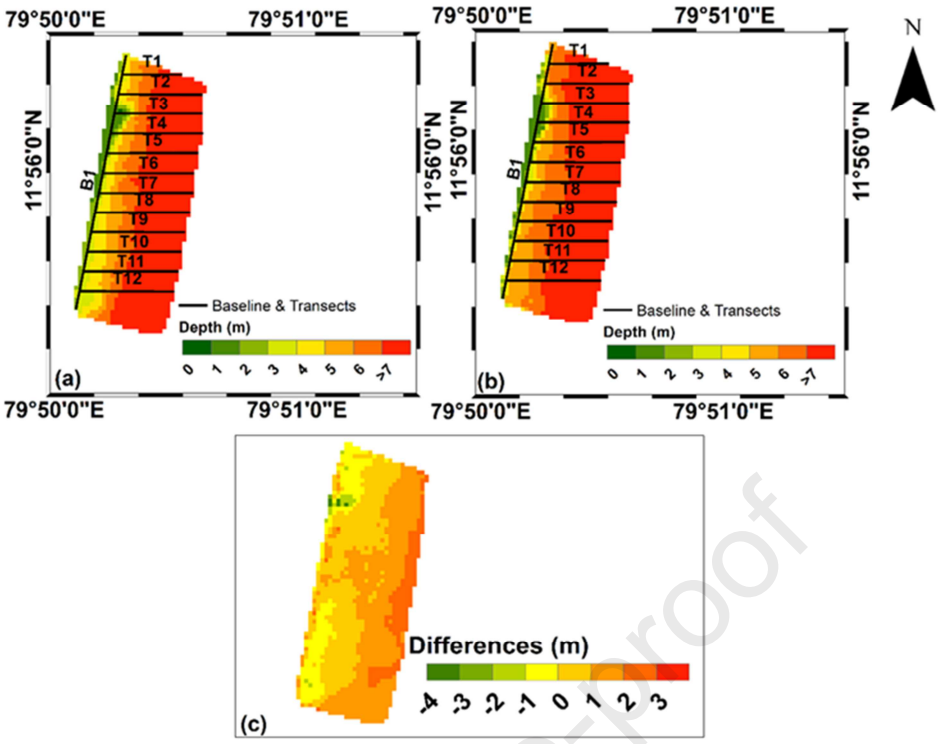

Figure 5 Comparison of bathymetry map obtained using (a) In-situ measurement (b) Landsat OLI imagery of October 2017 showing baseline B1 and transects (T1-T12) spaced every 150m

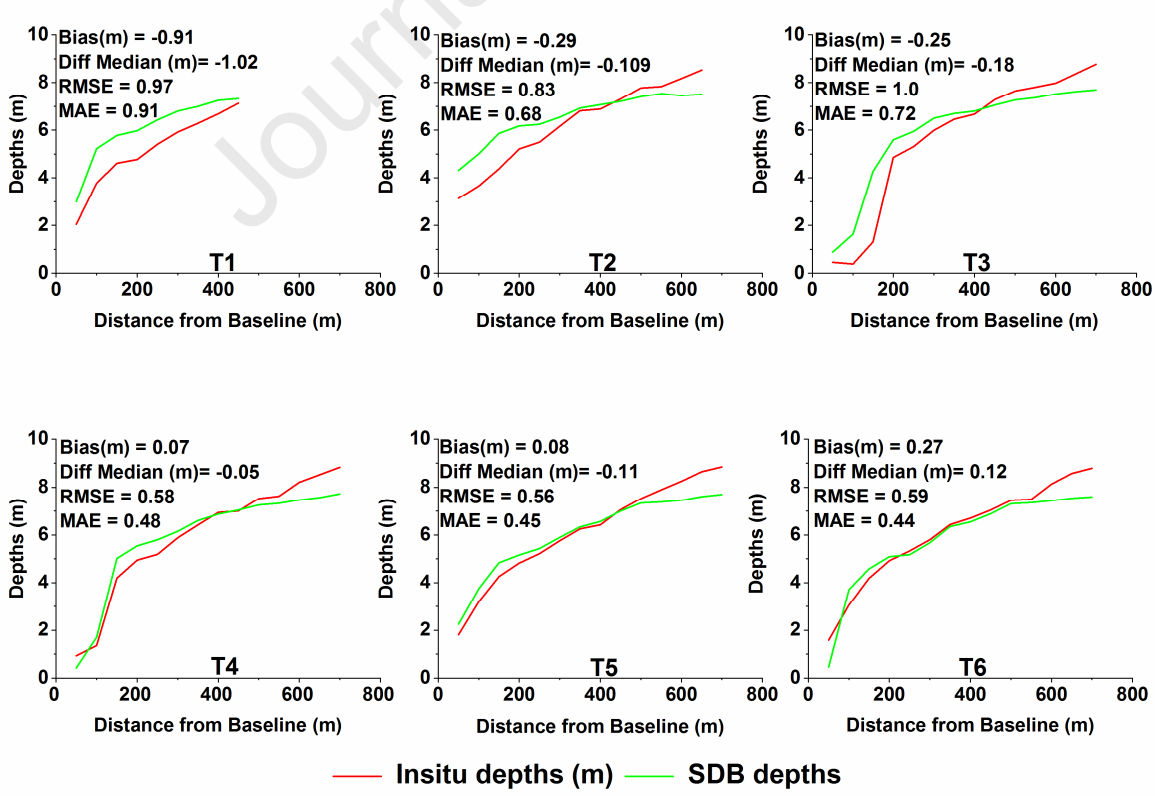

Figure 6 Comparison of near-shore seabed profiles of Oct 2017 for transects T1-T6

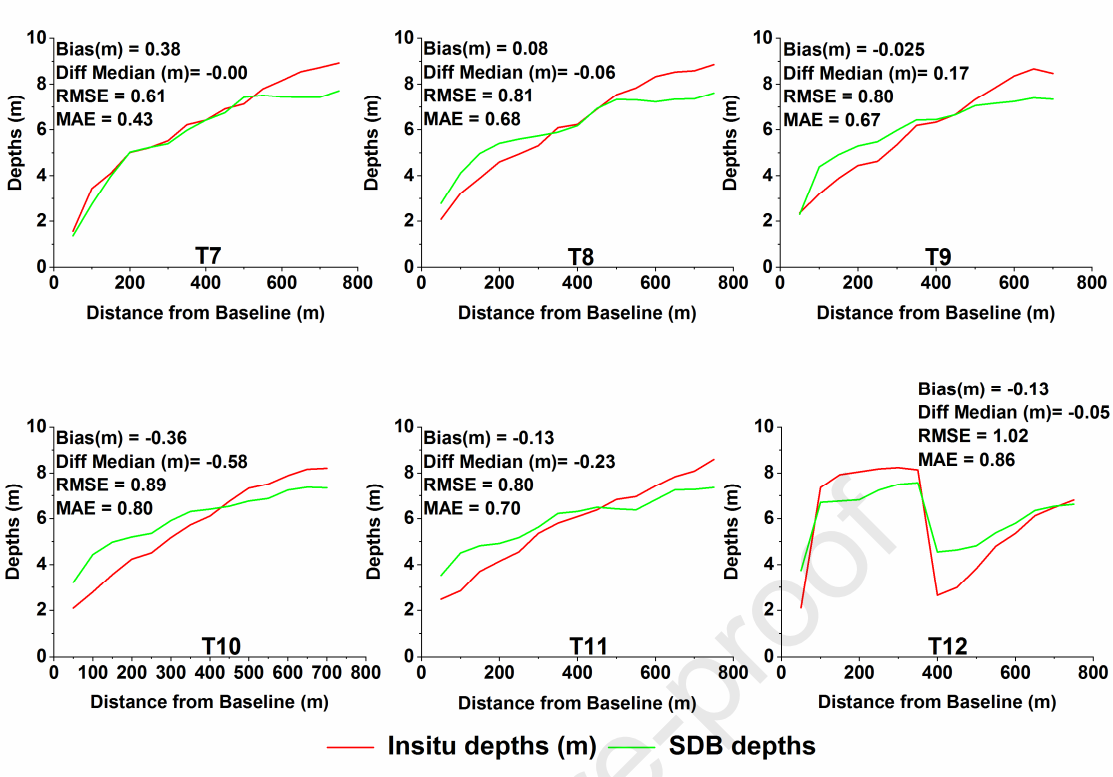

Figure 7 Comparison of near-shore seabed profiles of Oct 2017 for transects T7-T12

4.2 Geomorphological changes along the Puducherry coast

4.2.1 SDB based geomorphological change analysis

The multi-temporal depth maps obtained after rigorous calibration and validation as reported in the previous section are finally utilized to understand the geomorphological changes that have occurred in the region of Puducherry due to the beach restoration project. To the knowledge of the authors, this study is amongst the first that shows a practical application where SDBs are utilized for long-term coastal monitoring and assessment.

The construction of the Northern reef was started in May 2017 and was expected to be completed by July 2018 and the beach nourishment using approximately 3 lakh m3 of the dredged sand was implemented through pipeline nourishment for nearshore profiles and rainbow nourishment in case of offshore profiles. The various phases of beach nourishment carried out in this region, between Feb 2017 to Aug 2017, are listed in

Table 8, wherein in most cases, the point of nourishment is located near the pier.

In order to understand the geomorphological changes that have taken place, the temporal variation of nearshore SDB along a 3km stretch of Puducherry coastline before, during (March-October 2017) the restoration process is assessed. To accomplish this, four SDB maps of different months, February 2017, March 2017, October 2017 and January 2018 are compared (Figure 8) wherein the bathymetry map of January 2018 is obtained using the validated SVR model, although no in-situ measurements are available for this date. A gradual shallowing of depths is witnessed from May 2017 to Oct 2017, especially in the northern part of the shoreline, with respect to the pier location, highlighting the resultant growth of a beach in this coastal stretch. The beach appears to be stable even in January 2018, and hence, based on the visual inspection of the depths maps it can be clearly inferred that the beach restoration process has indeed led to positive alterations in the geomorphology of this region.

Table 8 Phases of beach nourishment carried out by National Institute of Ocean Technology (NIOT) (Source: NIOT, 2017)

S.No.	Description of survey	Period of nourishment	Quantity of sand (m^3)	Remarks
1	Pre Bathymetry Survey	06-01-2017	0	
2	1st Post Bathymetry Survey	23-02-2017	34314	Sand deposition on shore and beginning of wedge reef construction
3	2nd Post Bathymetry Survey	13-03-2017	11718	Sand deposition in Sea near pier
4	3rd Post	22-05-2017	29424	Sand deposition in Sea near pier

	Bathymetry Survey			
5	4th Post Bathymetry Survey	02-06-2017	51447	Sand deposition in Sea near pier
6	5th Post Bathymetry Survey	02-07-2017	73696	Sand deposition in Sea near pier
7	6th Post Bathymetry Survey	27-07-2017	93856	Sand deposition in Sea near pier
8	7th Post Bathymetry Survey	18-08-2017	12578	Sand deposition in Sea near pier and tentative completion of reef
	Grand Total		307033	

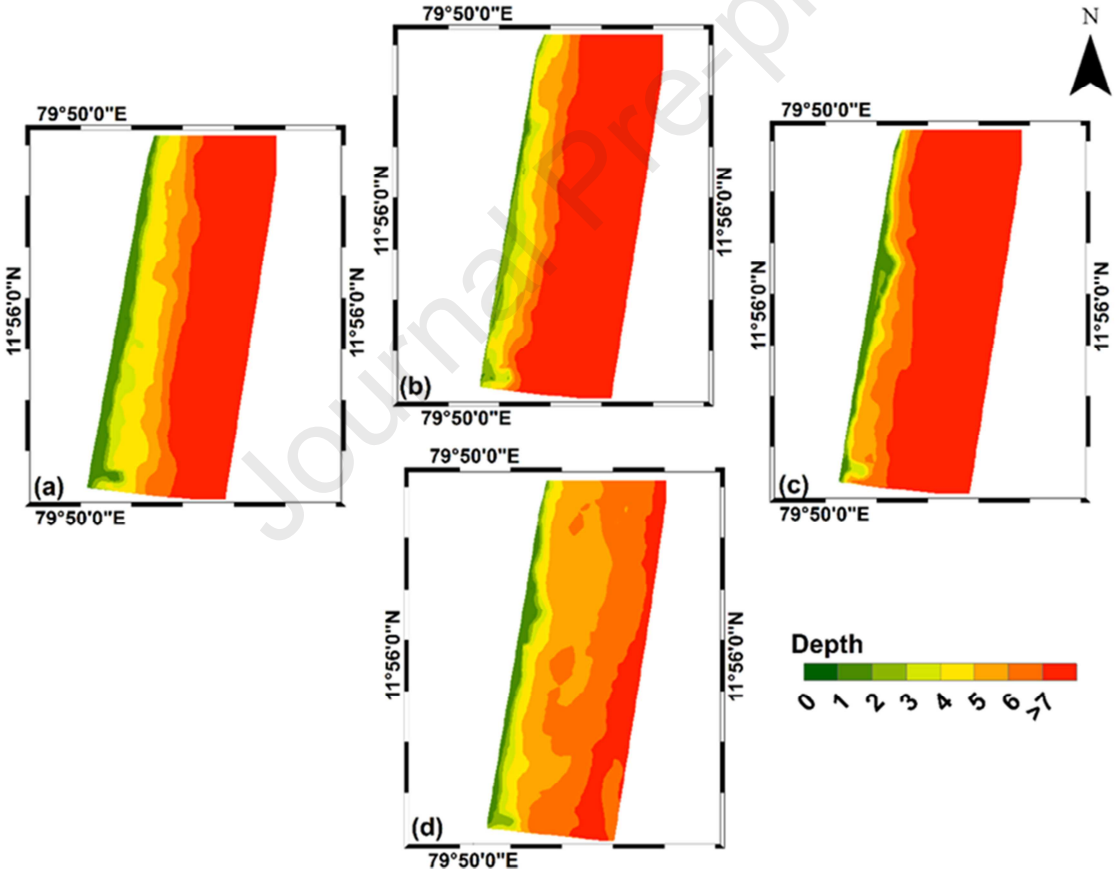

Figure 8 SDBs for the months (a) February 2017 (b) May 2017 (c) October 2017 (d) January 2018

This is further corroborated by Figure 9 and Figure 10 that show the difference in SDBs of the different months considered and the respective sediment volume changes. Here, the positive values indicate shallowing or accretion and the negative values depict deepening or

erosion. Negligible changes in bathymetry and volume are observed between Feb 2017 and May 2017 as the beach nourishment is reported to have begun during late February 2017. However, the difference between May 2017 and October 2017 shows a considerable reduction in the depths along the coastline, especially in the northern portion where volume change of the order 2000 – 3000m^3 are observed. In the case of October 2017- January 2018, the Southern portion appears to be accreting more with negligible erosion in the northern portion. It is reported (Umesh et al., 2017) that the net monthly transport of sediments along this region is northerly from March to October with the highest transport occurring in May and September. This trend reverses and becomes Southerly in rest of the months with the maximum transport observed in November and December (Rajab and Thiruvenkatasamy, 2017). It is to be noted that this trend concurs with the sediment dynamics observed using SDBs of this study.

The difference maps show a northerly movement of sediments, during the period between May and October; and southerly movement, between October- January. Moreover, it can also be established that the construction of the reef has successfully enabled beach replenishment, as can be seen in the October-January difference map, where negligible bathymetry change is observed along the coastline and the volume changes appear to be between -500 to 500m^3, an indication of stabilization. It is evident that significant morphological changes have occurred by virtue of the beach nourishment and the SDBs are able to capture the sediment dynamics with considerable accuracy. Nevertheless, in order to further validate the accretion and erosion trends observed through the SVR generated depth maps, a shoreline change analysis is carried out, where the satellite images are used independently to study the changes in the morphology of this coastline.

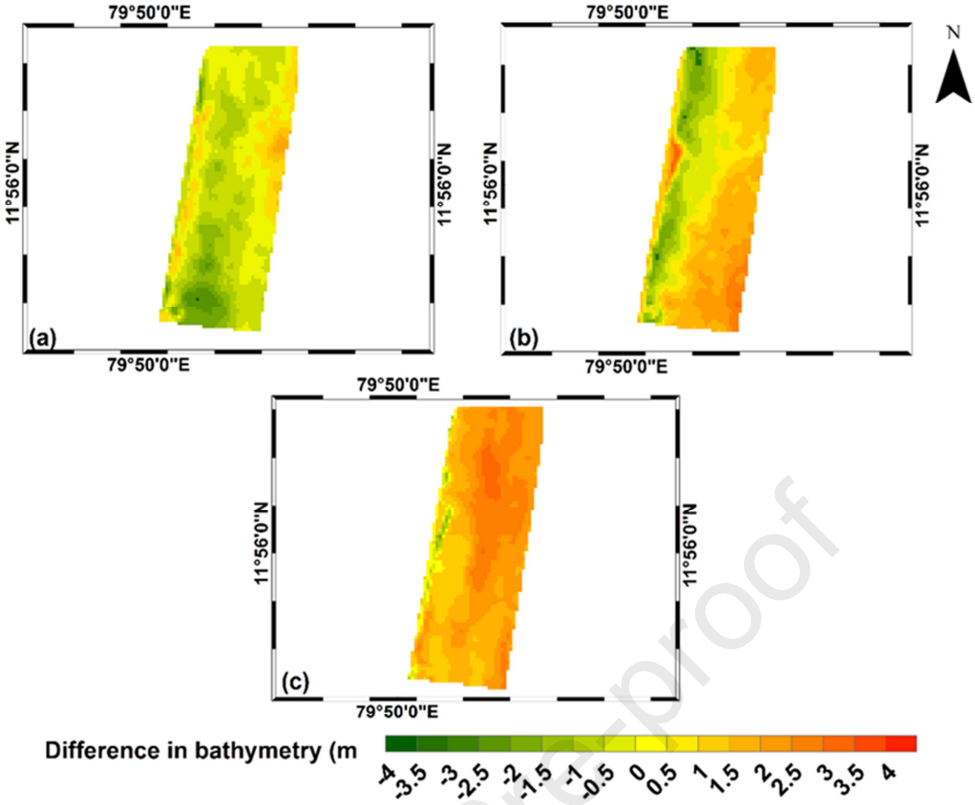

689

690 **Figure 9 Change in depths (a) Feb 2017- May 2017 (b) May 2017- Oct 2017 (c) Oct 2017**
691 **– January 2018**

692

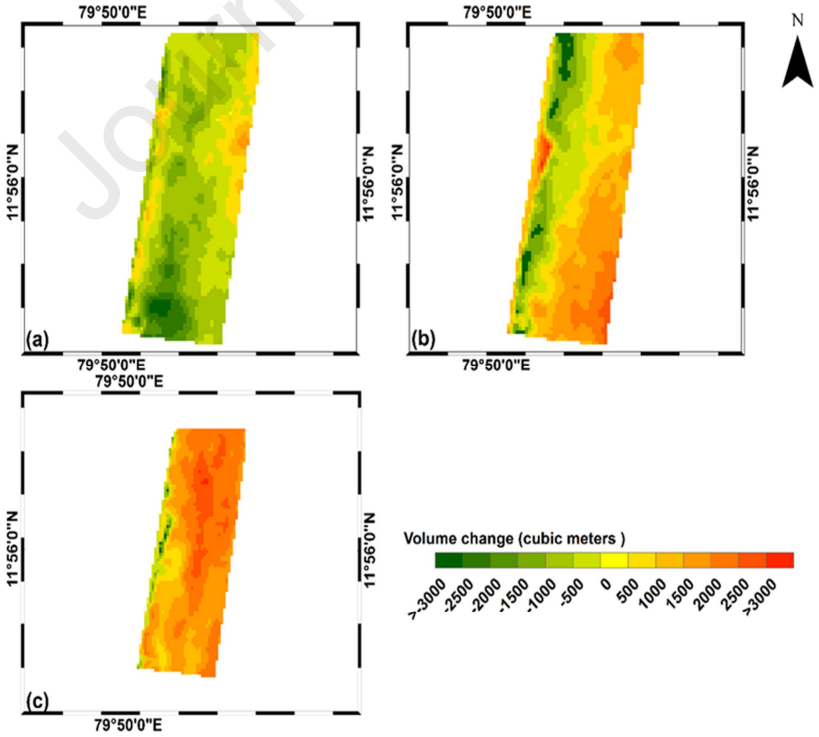

693

694 **Figure 10 Changes in sediment volume (a) February 2017- May 2017 (b) May 2017-**
695 **October 2017 (c) October 2017 – January 2018**

4.2.2 Digital shoreline change analysis

The accretion and erosion patterns in the region obtained from the DSAS based analysis can be observed in Figure 11.

In the case of February 2017- May 2017, about 83% of the transect points indicate erosion and about 17% show accretion. The average NSM and EPR estimated by considering all the transects is -13.68m and -3.42m/month respectively. The erosion and accretion pattern changes significantly when May 2017 and October 2017 are analysed for shoreline changes. About 53% of the shoreline is observed to be accreting and the rest 47% displays erosion. The average NSM is 7.7m and the EPR estimates are 1.2m/month. About 76% of the shoreline shows accretion and 24% shows erosion when October 2017 and January 2018 are considered. In this case, the average NSM is 7.3m and the EPR is 1.8m/month which is a marginal change from rates estimated for May-October 2017, which can again be possibly attributed to beach stabilization.

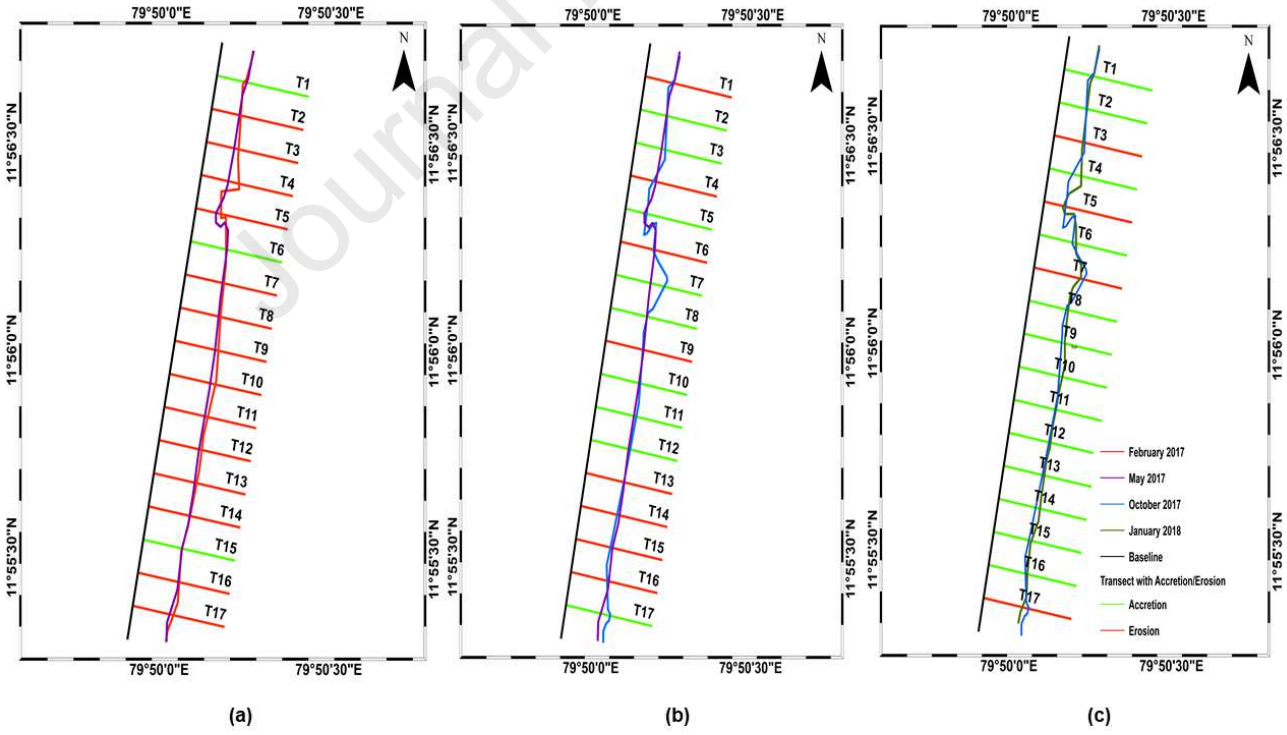

Figure 11 Shoreline changes (a) February 2017- May 2017 (b) May 2017- October 2017 (c) October 2017 – January 2018

Through this study as well, it can be deduced that the beach restoration process has successfully resulted in beach replenishment, which is observed as accretion in the case of most transects for the month of October. The results obtained through the DSAS analysis show similar patterns of accretion and erosion, as observed in the assessment of bathymetry changes using SDBs. Moreover, a higher number of accreting transects are seen in the northern portion of the shoreline in comparison to the southern portion during May 2017 and October 2017. This reverses when October 2017 and January 2018 are considered, where several southern transects become accreting. This observation agrees with the results of SDB analysis indicating the movements of sediments to be northern between May to October and Southern between November to February (Ramesh et al. 2011).

It can therefore be conclusively reported that the strategy of construction of reef as well as sand nourishment has proved to be a constructive process towards the restoration of beach along the Puducherry coastline in the period between 2017-2018. This shoreline is infamous for being severely eroding due to the construction of various shore protection structures, and it is imperative to take steps to arrest the loss of the beach which has immense ecosystem end economic value. From this perspective, this beach restoration project shows promising results as a mitigation measure for protecting the coastline in this region. The final validation of this study is presented in the annual report of NIOT, which mentions that a wide beach was formed between the chief's Secretary office to Gandhi statue. This is also seen in the bathymetry output for October 2017 which is overlapped on the google earth image in Figure 12.

738

739 **Figure 12 (a) SDB obtained for October 2017 overlapped on Google earth image (b)**
740 **Actual image of the widening of the beach (Source NIOT Annual Report 2017-18)**

741

742 ## 5. Conclusion

743 The study assesses the coastal geomorphological impact of a beach restoration project taken
744 up by the government to curb the shoreline erosion along the coast of Puducherry, India.
745 Landsat 8 OLI based depth maps derived by applying a non-linear regression-based machine
746 learning technique called Support Vector Regression (SVR) are used to conduct this analysis
747 and the results are further confirmed using a DSAS based shoreline change study. The statics
748 obtained on comparing the maps obtained from in-situ measurements and those from satellite
749 datasets; as well as the nearshore profiles demonstrate the capabilities of this approach for
750 shallow water depth estimation. The Low RMSE and MAE values for all the datasets also
751 highlight the importance of SDBs for multi-temporal coastal monitoring studies, where
752 carrying out repeated field measurements is a major limitation. This is also advantageous for
753 studies involving numerical modelling of coastal dynamics, where updated depth information
754 is required at varying spatial and temporal scales.
755 Further, the SDB based geomorphological analysis of the 3Km coastal stretch in Puducherry
756 provides valuable insights on the effect of the coastal protection measures carried out in this
757 region (construction of artificial reefs and beach nourishment).The analysis shows the growth
758 of a small patch of beach along the northern part of this coastal stretch as well as subsequent

stabilization of the coastline. The pattern of accretion and erosion observed in the SDBs are also witnessed through the shoreline changes analysis and both the methods successfully capture the monthly trends of sediment movement. It can thus be considered, that this mitigation measure is beneficial for the protection of this eroding coastline. The limitation in of this study is that the study is conducted only up to January 2018 due to the lack of in-situ measurement for validation. Nevertheless, this presents the future scope of this study, where the accuracy of model can be enhanced by including more field measurements both during training and testing.

Conclusively, this research is a unique attempt, to successfully utilize Satellite Derived Bathymetry to understand and monitor continental shelf sea dynamics, which is mostly difficult due to the constraints in procuring temporal field data. Bathymetry products from free medium resolution imageries of Landsat 8 OLI or Sentinel 2 MSI can ensure availability of depth information at reasonable resolutions to coastal scientists and managers thereby enabling a continuity in coastal research and management.

Acknowledgement

The authors thank National Institute of Ocean Technology (NIOT), Chennai, India for providing the echo-sounding measurements for the study region of Puducherry. We would also like to thank Dr. Roshanka Ranasinghe and Dr. Zoran Vojinovic for providing Ms. Ankita Misra with an opportunity to learn and understand the concept of Support Vector Machines at UNESCO- IHE, The Netherlands.

References

Benny, A.H. and Dawson, G.J., 1983. Satellite imagery as an aid to bathymetric charting in the Red Sea. The Cartographic Journal, 20(1), 5-16.

Bharathi, M. D., Patra, S., Sundaramoorthy, S., Madeswaran, P., & Sundaramanickam, A. 2017. Elucidation of seasonal variations of physicochemical and biological parameters with statistical analysis methods in Puducherry coastal waters. Marine pollution bulletin, 122(1-2), 432-440.

Bierwirth, P.N., Lee, T.J. and Burne, R.V., 1993. Shallow sea-floor reflectance and water depth derived by unmixing multispectral imagery. Photogrammetric Engineering and Remote Sensing;(United States), 59(3).

Brando, V. E., Anstee, J. M., Wettle, M., Dekker, A. G., Phinn, S. R., & Roelfsema, C. 2009. A physics based retrieval and quality assessment of bathymetry from suboptimal hyperspectral data. Remote Sensing of Environment, 113(4), 755-770.

Cahalane, C., Magee, A., Monteys, X., Casal, G., Hanafin, J. and Harris, P., 2019. A comparison of Landsat 8, RapidEye and Pleiades products for improving empirical predictions of satellite-derived bathymetry. Remote sensing of environment, 233, 111414.

Casella, E., Collin, A., Harris, D., Ferse, S., Bejarano, S., Parravicini, V., ... & Rovere, A. 2017. Mapping coral reefs using consumer-grade drones and structure from motion photogrammetry techniques. Coral Reefs, 36(1), 269-275.

Ceyhun, Ö., & Yalçın, A. 2010. Remote sensing of water depths in shallow waters via artificial neural networks. Estuarine, Coastal and Shelf Science, 89(1), 89-96.

Chirayath, V., & Earle, S. A. 2016. Drones that see through waves–preliminary results from airborne fluid lensing for centimetre-scale aquatic conservation. Aquatic Conservation: Marine and Freshwater Ecosystems, 26, 237-250.

Collin, A. and Hench, J.L., 2015. Extracting shallow bathymetry from very high resolution satellite spectral bands and a machine learning algorithm. International Council of the Exploration of the Sea (ICES) CM, 24.

Danilo, C., & Melgani, F. (2016). Wave period and coastal bathymetry using wave propagation on optical images. IEEE Transactions on Geoscience and Remote Sensing, 54(11), 6307-6319.

Danilo, C. and Melgani, F., 2019. High-coverage satellite-based coastal bathymetry through a fusion of physical and learning methods. Remote Sensing, 11(4), p.376.

Deidda, M., & Sanna, G. 2012. Pre-processing of high-resolution satellite images for sea bottom classification. Italian Journal of Remote Sensing/Rivista Italiana di Telerilevamento, 44(1)

Doxani, G., Papadopoulou, M., Lafazani, P., Pikridas, C., & Tsakiri-Strati, M. 2012. Shallow-water bathymetry over variable bottom types using multispectral Worldview-2 image. International Archives of the Photogrammetry, Remote Sensing and Spatial Information Sciences, 39(8), 159-164.

El Kafrawy, S.B., Basiouny, M.E., Ghanem, E.A., and Taha, A.S., 2017. Performance Evaluation of Shoreline Extraction Methods Based on Remote Sensing Data. Journal of Geography, Environment and Earth Science International, 11(4), 1-18,

Eugenio, F., Marcello, J., & Martin, J. 2015. High-resolution maps of bathymetry and benthic habitats in shallow-water environments using multispectral remote sensing imagery. IEEE Transactions on Geoscience and Remote Sensing, 53(7), 3539-3549.

Gao, J., 2009. Bathymetric mapping by means of remote sensing: methods, accuracy and limitations. Progress in Physical Geography, 33(1), 103-116.

Geyman, E. C., & Maloof, A. C. 2019. A simple method for extracting water depth from multispectral satellite imagery in regions of variable bottom type. Earth and Space Science, 6(3), 527-537.

Gholamalifard, M., Esmaili Sari, A., Abkar, A., & Naimi, B. 2013. Bathymetric modeling from satellite imagery via single band algorithm (SBA) and principal components analysis (PCA) in southern Caspian Sea. International journal of environmental research, 7(4), 877-886.4

Hamylton, S.M., Hedley, J.D. and Beaman, R.J., 2015. Derivation of high-resolution bathymetry from multispectral satellite imagery: A comparison of empirical and optimisation methods through geographical error analysis. Remote Sensing, 7(12), pp.16257-16273.

Hedley, J., Russell, B., Randolph, K., & Dierssen, H. 2016. A physics-based method for the remote sensing of seagrasses. Remote sensing of environment, 174, 134-147.

Jawak, S. D., Vadlamani, S. S., & Luis, A. J., 2015. A synoptic review on deriving bathymetry information using remote sensing technologies: models, methods and comparisons. Advances in Remote Sensing, 4(02), 147.

Jawak, S. D., & Luis, A. J., 2015. Spectral information analysis for the semiautomatic derivation of shallow lake bathymetry using high-resolution multispectral imagery: A case study of Antarctic coastal oasis. Aquatic Procedia, 4, 1331-1338.

Jupp, D. L. B. 1988. Background and extensions to depth of penetration (DOP) mapping in shallow coastal waters. In Proceedings of the Symposium on Remote Sensing of the Coastal Zone (pp. IV-2).

Kabiri, K., 2017. Accuracy assessment of near-shore bathymetry information retrieved from Landsat-8 imagery. Earth Science Informatics, 10(2),

235-245.

Kerr, J. M., & Purkis, S. 2018. An algorithm for optically-deriving water depth from multispectral imagery in coral reef landscapes in the absence of ground-truth data. Remote sensing of environment, 210, 307-324.

Knudby, A., Ahmad, S.K. and Ilori, C., 2016. The potential for Landsat-based bathymetry in Canada. Canadian Journal of Remote Sensing, 42(4), 367-378.

Kudale, M. D., Kanetkar, C. N., & Poonawala, I. Z. 2004. Design wave prediction along the coast of India. In Proceedings of the 3rd Indian National Conference on Harbour and Ocean Engineering, NIO, Goa, 1, 31-38.

Lafon, V., Froidefond, J.M., Lahet, F. and Castaing, P., 2002. SPOT shallow water bathymetry of a moderately turbid tidal inlet based on field measurements. Remote sensing of Environment, 81(1), 136-148.

Lee, Z., Carder, K.L., Mobley, C.D., Steward, R.G. and Patch, J.S., 1999. Hyperspectral remote sensing for shallow waters: 2. Deriving bottom depths and water properties by optimization. Applied optics, 38(18), 3831-3843.

Legleiter, C. J., Roberts, D. A., & Lawrence, R. L. 2009. Spectrally based remote sensing of river bathymetry. Earth Surface Processes and Landforms, 34(8), 1039-1059.

Liu, S., Gao, Y., Zheng, W., & Li, X. 2015. Performance of two neural network models in bathymetry. Remote sensing letters, 6(4), 321-330.

Liew, S. C., Chang, C. W., & Kwoh, L. K., 2012. Sensitivity Analysis in the Retrieval of Turbid Coastal Water Bathymetry Using WorldView-2 Satellite Data. International Archives of the Photogrammetry, Remote Sensing and Spatial Information Sciences, Volume XXXIX-B7, XXII ISPRS Congress, 25 August – 01 September 2012, Melbourne, Australia

Lyzenga, D. R. 1978. Passive remote sensing techniques for mapping water depth and bottom features. Applied optics, 17(3), 379-383.

Lyzenga, D.R. 1981. Remote sensing of bottom reflectance and water attenuation parameters in shallow water using aircraft and Landsat data." International journal of remote sensing, 2(1): 71-82.

Lyzenga, D. R., Malinas, N. P., & Tanis, F. J., 2006. Multispectral bathymetry using a simple physically based algorithm. IEEE Transactions on Geoscience and Remote Sensing, 44(8), 2251-2259.

Ma, H., Guo, S., & Zhou, Y. 2013. Detection of water area change based on remote sensing images. In Geo-Informatics in Resource Management and Sustainable Ecosystem (pp. 626-636). Springer, Berlin, Heidelberg.

Makboul, O., Negm, A., Mesbah, S., & Mohasseb, M. 2017. Performance assessment of ANN in estimating remotely sensed extracted bathymetry. Case study: Eastern harbor of alexandria. Procedia Engineering, 181, 912-919.

Mancini, S., Olsen, R.C., Abileah, R. and Lee, K.R., 2012, May. Automating nearshore bathymetry extraction from wave motion in satellite optical imagery. In Algorithms and Technologies for Multispectral, Hyperspectral, and Ultraspectral Imagery XVIII (Vol. 8390, p. 83900P). International Society for Optics and Photonics.

Maritorena, S., Morel, A., & Gentili, B. 1994. Diffuse reflectance of oceanic shallow waters: Influence of water depth and bottom albedo. Limnology and oceanography, 39(7), 1689-1703.

Martens, H. A., & Dardenne, P. 1998. Validation and verification of regression in small data sets. Chemometrics and intelligent laboratory systems, 44(1-2), 99-121.

Mishra, M. K., Ganguly, D., & Chauhan, P. 2013. Estimation of coastal bathymetry using RISAT-1 C-band microwave SAR data. IEEE Geoscience and Remote Sensing Letters, 11(3), 671-675.

Misra, A., Vojinovic, Z., Ramakrishnan, B., Luijendijk, A., & Ranasinghe, R. 2018. Shallow water bathymetry mapping using Support Vector Machine (SVM) technique and multispectral imagery. International journal of remote sensing, 39(13), 4431-4450.

Misra, A., Ramakrishnan, B., Vojinovic, Z., Luijendijk, A., & Ranasinghe, R. 2019. Assessment of Complementary Medium-Resolution Satellite Imageries for Nearshore Bathymetry Estimation. Journal of the Indian Society of Remote Sensing, 47(3), 537-540.

Mobley, C. D., Werdell, J., Franz, B., Ahmad, Z., & Bailey, S. 2016. Atmospheric correction for satellite ocean color radiometry.

Mohamed, H., Salah, M., Nadaoka, K. and Zahran, M., 2017. Assessment of proposed approaches for bathymetry calculations using multispectral satellite images in shallow coastal/lake areas: a comparison of five models. Arabian Journal of Geosciences, 10(2), 42.

Mohammad, S., Kiritchenko, S., Sobhani, P., Zhu, X., & Cherry, C. (2016, June). Semeval-2016 task 6: Detecting stance in tweets. In Proceedings of the 10th International Workshop on Semantic Evaluation (SemEval-2016) (pp. 31-41)

Neelamani, S., & Sundaravadivelu, R. 2006. Erosion, protection of Pondicherry coast, southeast India. Journal of Coastal Research Special, (39), 880-883.

Niroumand-Jadidi, M., Vitti, A., & Lyzenga, D. R. 2018. Multiple Optimal Depth Predictors Analysis (MODPA) for river bathymetry: Findings from spectroradiometry, simulations, and satellite imagery. Remote sensing of environment, 218, 132-147.

Pacheco, A., Horta, J., Loureiro, C. and Ferreira, Ó., 2015. Retrieval of nearshore bathymetry from Landsat 8 images: A tool for coastal monitoring in shallow waters. Remote Sensing of Environment, 159, 102-116.

Pahlevan, N., Lee, Z., Wei, J., Schaaf, C. B., Schott, J. R., & Berk, A. 2014. On-orbit radiometric characterization of OLI (Landsat-8) for applications in aquatic remote sensing. Remote Sensing of Environment, 154, 272-284.

Philpot, W. D., 1989. Bathymetric mapping with passive multispectral imagery. Applied optics, 28(8), 1569-1578.

Pleskachevsky, A., Lehner, S., Heege, T. and Mott, C., 2011. Synergy and fusion of optical and synthetic aperture radar satellite data for underwater topography estimation in coastal areas. Ocean Dynamics, 61(12), pp.2099-2120.

Purkis, S. J. 2018. Remote sensing tropical coral reefs: The view from above. Annual Review of Marine Science, 10, 149-168.

Pushparaj, J. and Hegde, A.V., 2017. Estimation of bathymetry along the coast of Mangaluru using Landsat-8 imagery. The International Journal of Ocean and Climate Systems, 8(2), 71-83.

Rajab, P. M., & Thiruvenkatasamy, K. (2017). Estimation of longshore sediment transport along Puducherry coast, Eastcoast of India; based on empirical methods and surf zone model.Indian Journal of Geo Marine Sciences,46 (07),1307-1319.

995 Ramesh, R., Purvaja, R., & Senthil Vel, A., 2011. National assessment of shoreline change:
996 puducherry coast. NCSCM/MoEF report, 1, 57 pp.
997
998 Rana, M., & Koprinska, I. (2016). Neural network ensemble based approach for 2D-interval
999 prediction of solar photovoltaic power. Energies, 9(10), 829.
1000
1001 Sagawa, T., Yamashita, Y., Okumura, T. and Yamanokuchi, T., 2019. Satellite Derived
1002 Bathymetry Using Machine Learning and Multi-Temporal Satellite Images. Remote
1003 Sensing, 11(10), 1155.
1004
1005 Sandhya, K.G., Nair, T.B., Bhaskaran, P.K., Sabique, L., Arun, N. and Jeykumar, K. (2014).
1006 Wave forecasting system for operational use and its validation at coastal Puducherry, east
1007 coast of India. Ocean Engineering, 80, 64-72.
1008
1009 Selvan, S. C., Kankara, R. S., Markose, V. J., Rajan, B., & Prabhu, K. (2016). Shoreline
1010 change and impacts of coastal protection structures on Puducherry, SE coast of India. Natural
1011 Hazards, 83(1), 293-308.
1012
1013 Smola, A. J., & Schölkopf, B., 2004. A tutorial on support vector regression. Statistics and
1014 computing, 14(3), 199-222.
1015
1016 Solomatine, D., See, L.M. and Abrahart, R.J., 2009. Data-driven modelling: concepts,
1017 approaches and experiences. In Practical hydroinformatics (pp. 17-30). Springer, Berlin,
1018 Heidelberg.
1019
1020 Spitzer, D., & Dirks, R. W. J. (1986). Classification of bottom composition and bathymetry
1021 of shallow waters by passive remote sensing. In: Remote sensing for resources development
1022 and environmental management; Proceedings of the Seventh International Symposium,
1023 Enschede, Netherlands, Aug. 25-29, 2, 775-777.
1024
1025 Stauble, D.K. (1998). Techniques for measuring and analyzing inlet ebb-shoal evolution (No.
1026 CETN-IV-13). Engineer Research and Development Center, Vicksburg Ms Coastal and
1027 Hydraulics Lab.
1028

Stumpf, R. P., Holderied, K., & Sinclair, M., 2003. Determination of water depth with high-resolution satellite imagery over variable bottom types. Limnology and Oceanography, 48(1part2), 547-556.

Thieler, E.R., Himmelstoss, E.A., Zichichi, J.L. and Miller, T.L., 2005. Digital Shoreline Analysis System (DSAS) Version 3.0: an Arcgis extension for calculating shoreline change. United States Geological Survey, Open File Report 2005–1304.

Traganos, D., Poursanidis, D., Aggarwal, B., Chrysoulakis, N. and Reinartz, P., 2018. Estimating satellite-derived bathymetry (SDB) with the google earth engine and sentinel-2. Remote Sensing, 10(6), 859.

Umesh, P.A., Bhaskaran, P.K., Sandhya, K.G. and Nair, T.B. (2017). An assessment on the impact of wind forcing on simulation and validation of wave spectra at coastal Puducherry, east coast of India. Ocean Engineering, 139, 14-32.

Vapnik, V.N., 1995. The Nature of Statistical L earning T heory. New York: Springer2V erlag.

Van Rijn, L. C. (2011). Coastal erosion and control. Ocean & Coastal Management, 54(12), 867-887.

Vanhellemont, Q., & Ruddick, K. (2014). Landsat-8 as a precursor to Sentinel-2: Observations of human impacts in coastal waters. ESA Special Publication, 726.

Vanhellemont, Q., & Ruddick, K. (2015). Advantages of high quality SWIR bands for ocean colour processing: Examples from Landsat-8. Remote Sensing of Environment, 161, 89-106.

Vanhellemont, Q., & Ruddick, K. (2016). Acolite for Sentinel-2: Aquatic applications of MSI imagery. In Proceedings of the 2016 ESA Living Planet Symposium, Prague, Czech Republic (9-13).

Vanhellemont, Q., & Ruddick, K. (2018). Atmospheric correction of metre-scale optical satellite data for inland and coastal water applications. Remote Sensing of Environment, 216, 586-597.

Vanhellemont, Q. (2019). Adaptation of the dark spectrum fitting atmospheric correction for aquatic applications of the Landsat and Sentinel-2 archives. Remote Sensing of Environment, 225, 175-192.

Vinayaraj, P., Raghavan, V. and Masumoto, S., 2016. Satellite-derived bathymetry using adaptive geographically weighted regression model. Marine Geodesy, 39(6), 458-478.

Vojinovic, Z., Abebe, Y.A., Ranasinghe, R., Vacher, A., Martens, P., Mandl, D.J., Frye, S.W., Van Ettinger, E. and De Zeeuw, R., 2013. A machine learning approach for estimation of shallow water depths from optical satellite images and sonar measurements. Journal of Hydroinformatics, 15(4), 1408-1424.

Wang, L., Liu, H., Su, H. and Wang, J., 2019. Bathymetry retrieval from optical images with spatially distributed support vector machines. GIScience & remote sensing, 56(3), 323-337.

Yunus, A.P., Dou, J., Song, X. and Avtar, R., 2019. Improved bathymetric mapping of coastal and lake environments using Sentinel-2 and Landsat-8 images. Sensors, 19(12), 2788.

Zhihua, Y & Honglian, L., 2012. Based on Radial Basis Kernel Function of Support Vector Machines for Speaker Recognition Image and Signal Processing (CISP), 2012 5th International Congress on Image and Signal Processing, Chongqing, China, 1584 - 1587.

http://www.ceehydrosystems.com/products/single-beam-echo-sounders/cee echo/#1511901053278-fdfe7119-b0bb

https://www.niot.res.in/documents/admin_press_release/Bringing_Puducherry_Livemint.pdf

http://environmentclearance.nic.in/writereaddata/online/RiskAssessment/14082016FMP8ZW9Itask2_design.pdf

https://www.niot.res.in/documents/admin_annual_report/Annual_report-2017-18.pdf

- Ratio based single predictor driven SVM performs well for depth estimation
- Low RMSE of <1m is achieved in case of all Multi-date imageries used
- Depth maps obtained from SVM can be used for coastal geomorphological analysis.
- Satellite bathymetry an effective alternative to repeated in-situ surveys

This manuscript has not been published and is not under consideration for publication elsewhere. We have no conflicts of interest to disclose.